Rev. Roum. Sci. Techn.– Électrotechn. et Énerg.
Vol. **70**, *3*, pp. 385–390, Bucarest, 2025

ADAPTIVE SYNERGETIC AND LONG-RANGE COMMUNICATION LORA FOR QUADROTOR CONTROL AND INDOOR LOCALIZATION VIA INTERVAL ANALYSIS

FAWZI SRAIRI [1], KHALIL MOKHTARI [2], KHEIREDDINE CHARA [1], KAMEL SRAIRI [3], MOHAMED BENBOUZID [4, 5, *]

Keywords: Adaptive synergetic; Communication; Control; Indoor localization; Interval analysis; Long-range (LoRa); Quadrotor.

In this article, a new approach based on the use of received signal strength indication (RSSI) combined with long-range (LoRa) communication technology has been developed to locate a drone. Additionally, an interval analysis was introduced to enhance localization accuracy and system reliability. This approach involves taking into account several RSSI measurements over defined time intervals. The quadrotor is controlled by an adaptive control system based on the passivity of the system's ASC. By combining RSSI with LoRa technology, interval analysis, and passivity-based ASC control, our approach offers a robust and efficient solution for UAV control and localization. This methodology could be applied in a multitude of real-life scenarios, offering significant benefits in terms of safety, operational efficiency, and overall performance of UAV systems.

1. **INTRODUCTION**

Recently, advances in wireless communications for unmanned aerial vehicles (UAV) have opened up vast navigation horizons, making navigation fully autonomous in both outdoor and indoor environments. UAVs have missions in a wide range of sectors, including monitoring, logistics, and agriculture. Some applications, such as facility monitoring, inspection, and warehouse management, are critical in terms of time and security of information on the quadrotor's position. Sudden changes in the environment and missions in indoor environments typically require a high degree of precision, necessitating the real-time estimation of the drone's position [1].

Although there are research works based on advanced techniques in the field of UAV localization, [2] has developed an integrated system using an on-board convolutional neural network (CNN) to estimate the relative position between nano-UAVs, with a low-resolution camera and a very low-power system-on-chip. However, this method is constrained by the limited resources on board the nano-UAVs, which can restrict the complexity of the algorithms deployed, and it depends on the performance of the deep learning models under real flight conditions.

Additionally, [3] proposes a passive drone localization and detection system based on radio frequencies (RF), utilizing angle-of-arrival (AoA) and triangulation techniques. However, the proposed method has limitations, including a dependence on the accuracy of rotating antennas and software-defined radios (SDRs), which can affect reliability in complex environments.

Additionally, [4] focuses on a framework for detecting and identifying drone controller signals using the frequency-hopping spread spectrum (FHSS) technique and estimating their direction of arrival using a uniform linear antenna array. However, the method has high complexity due to cyclostationary analysis and the short-time Fourier transform, as well as sensitivity to nonlinear viewing environments, which can affect the accuracy of direction estimates.

In this paper, we propose a novel approach to UAV control and localization that utilizes RSSI in conjunction with LoRa communication technology. RSSI, which measures the strength of the radio signal received by the drone from ground stations, is used to estimate the distance between the drone and these ground reference points by combining RSSI with LoRa technology, which offers extended range and robust communication over long distances.

Additionally, we are introducing interval analysis to enhance localization accuracy and system reliability. This approach involves collecting and analyzing multiple RSSI measurements over defined time intervals to extrapolate the drone's current position with greater accuracy. By considering signal fluctuations over specified periods, our method can compensate for inaccuracies due to environmental factors.

Complementing this localization approach, the quadrotor is controlled by an adaptive controller based on the system's passivity. Unlike conventional controllers, which often struggle to maintain optimum performance in the face of varying environmental conditions, our method exploits the passive properties of the system to ensure robust stabilization of the quadrotor, even in complex and disturbed environments.

The primary advantage of this controller lies in its ability to adapt in real-time to external disturbances, ensuring enhanced asymptotic stability and robustness. This approach overcomes the limitations of traditional static controllers, which can fail under dynamic conditions. By incorporating interval analysis and accounting for signal fluctuations over specific periods, our method not only improves localization accuracy but also enhances flight stability, providing a more reliable solution for Quadrotor control during localization.

2. **PRELIMINARIES**

2.1 QUADROTOR MATHEMATICAL MODELING

The architecture of the LoRa drone localization system is based on an approach designed to optimize localization accuracy, robustness, and energy efficiency. This

[1] LAAAS, Department of Electronics, University of Batna 2, Batna 05000, Algeria.
[2] Department of Electrical Engineering, University Abbes Laghrour of Khenchela, Khenchela 40004, Algeria.
[3] LMSE Laboratory, Department of Electrical Engineering, University of Biskra, BP 145, Biskra 07000, Algeria.
[4] University of Brest, Institut de Recherche Dupuy de Lôme (UMR CNRS 6027 IRDL), 29238 Brest, France.
[5,] Shanghai Maritime University, Logistics Engineering College, Shanghai 201306, China.(correspondence)
Emails: fawzi.srairi@univ-batna2.dz, k.chara@univ-batna2.dz, khalil.mokhtari@univ-khenchela.dz, k.srairi@univ-biskra.dz, mohamed.benbouzid@univ-brest.fr

DOI: 10.59277/RRST-EE.2025.70.3.17

architecture, comprising three interdependent elements—the drone to be localized, the LoRa beacons, and the base station—forms a coherent, scalable ecosystem. The drone is equipped with LoRa communication modules. This module enables the drone to engage in bidirectional exchanges with LoRa beacons. The data exchanged includes not only the drone's current position, but also information on its status, speed, and other relevant parameters.

The base station is the brain of the localization system. It receives the signals emitted by the UAVs and beacons, collecting the raw data needed to calculate the precise position of the UAV. The considered body fixed frame B and the earth fixed frame E are shown in Fig. 1. The motion equations of the Quadrotor may be determined by combining the kinematics and dynamics models of the Quadrotor [1, 5–15]:

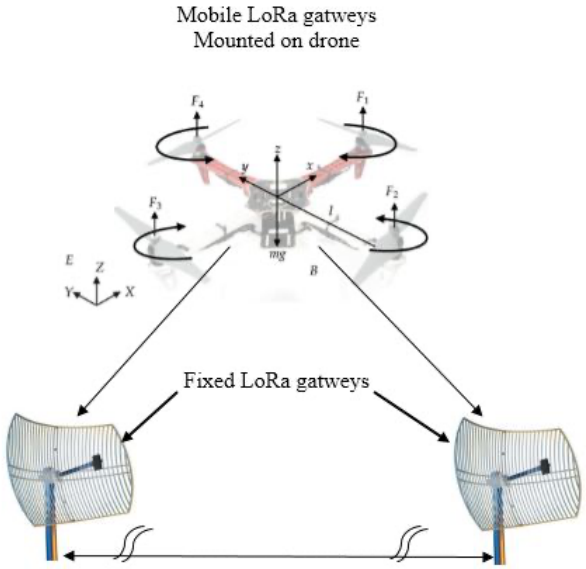

Fig. 1 – Quadrotor configuration with LoRa antennas: a body fixed frame B and earth frame E.

$$\begin{cases} \ddot{\phi} = \dot{\theta}\dot{\psi}\left(\frac{I_y - I_z}{I_x}\right) - \frac{J_r}{I_x}\dot{\theta}\Omega_r + \frac{l}{I_x}u_2 \\ \ddot{\theta} = \dot{\phi}\dot{\psi}\left(\frac{I_z - I_x}{I_y}\right) + \frac{J_r}{I_y}\dot{\phi}\Omega_r + \frac{l}{I_y}u_3 \\ \ddot{\psi} = \dot{\phi}\dot{\theta}\left(\frac{I_x - I_y}{I_z}\right) + \frac{1}{I_z}u_4 \\ \ddot{x} = -\frac{u_1}{m}(\cos\phi\sin\theta\cos\psi + \sin\phi\sin\psi) \\ \ddot{y} = -\frac{u_1}{m}(\cos\phi\sin\theta\sin\psi - \sin\phi\cos\psi) \\ \ddot{z} = g - \frac{u_1}{m}(\cos\phi\cos\theta) \end{cases} \quad (1)$$

where u_1, u_2, u_3, and u_4 are the control inputs, which can be calculated by: $u_1 = b(\Omega_1^2 + \Omega_2^2 + \Omega_3^2 + \Omega_4^2), u_2 = b(-\Omega_2^2 + \Omega_4^2), u_3 = b(\Omega_1^2 - \Omega_3^2)$, and $u_4 = d(\Omega_1^2 - \Omega_2^2 + \Omega_3^2 - \Omega_4^2)$, respectively. ϕ, θ, ψ, x, y and z stand for roll angles, pitch angle, yaw angle, x-position, y-position, and z-position, respectively. J_r is rotor inertia, I_x, I_y, I_z,are body-axis inertias, b is the thrust coefficient, d is the drag coefficient, l is a lever and $\Omega_r = \Omega_1 - \Omega_2 + \Omega_3 - \Omega_4$.

3. ADAPTIVE SYNERGETIC CONTROLLER FOR THE QUADROTOR SYSTEM

The following nonlinear state-space model can represent the dynamics of the Quadrotor:

$$\begin{aligned} \dot{x}(t) &= f\big(x(t), u(t)\big) = A(x)x(t) + B(x)u(t), \\ y(t) &= h\big(x(t)\big) = Cx(t), \end{aligned} \quad (2)$$

where $x(t) \in \mathbb{R}^n$ captures the system states, $u(t) \in \mathbb{R}^m$ denotes the control inputs, and $y(t) \in \mathbb{R}^m$ represents the measured outputs. The state transition matrices $A(x) \in \mathbb{R}^{n\times n}$ and $B(x) \in \mathbb{R}^{n\times m}$, along with the output matrix $C \in \mathbb{R}^{m\times n}$, do not need to be explicitly defined for implementing the proposed adaptive controller [15,16]. To meet the ASP requirements for the ASC method, an augmentation using a PFC (Parallel Feedforward Compensator) of the following form is introduced:

$$\begin{aligned} \dot{x}_f(t) &= A_f x_f(t) + B_f u(t), \\ y_f(t) &= C_f x_f(t), \end{aligned} \quad (3)$$

where $A_f = \operatorname{diag}\left(a_{f_1}, \dots, a_{f_m}\right) \in \mathbb{R}^{m\times m}$, $B_f = \operatorname{diag}\left(b_{f_1}, \dots, b_{f_m}\right) \in \mathbb{R}^{m\times m}$, and $C_f = \operatorname{diag}\left(c_{f_1}, \dots, c_{f_m}\right) \in \mathbb{R}^{m\times m}$. The elements c_{f_i} and b_{f_i} are positive for all $i = 1, \dots, m$. The augmented system is then given by:

$$\begin{aligned} \dot{x}_a(t) &= A_a(x_a)x_a(t) + B_a(x_a)u(t) \\ y_a(t) &= C_a x_a(t) \end{aligned} \quad (4)$$

where $x_a = \operatorname{col}\{x, x_f\} \in \mathbb{R}^{n_a}, y_a \in \mathbb{R}^m, A_a = \operatorname{diag}[A, A_f]$, $B_a = \operatorname{col}\{B, B_f\}$, and $C_a = [C, C_f]$.

The control development aims to achieve output tracking of an ideal linear reference model characterized by:

$$\begin{aligned} \dot{x}_m(t) &= A_m x_m(t) + B_m u_m(t) \\ y_m(t) &= C_m x_m(t) \end{aligned} \quad (5)$$

where $x(t) \in \mathbb{R}^{n_m}$ is the state vector of the model, $u_m(t) \in \mathbb{R}^{q_m}$ is the control input, and $y_m(t) \in \mathbb{R}^m$ represents the model's output signal. The matrices A_m, B_m, and C_m are appropriately dimensioned.

To define the control objective, the output tracking error $e_a(t) \in \mathbb{R}^m$ is specified as:

$$e_a(t) \triangleq y_m(t) - y_a(t). \quad (6)$$

The proposed adaptive synergetic control law takes the form [16]:

$$u_{ASC}(t) = K_e(t)e_a + K_x(t)x_m + K_u(t)u_m + K_s(t)x_a \quad (7)$$

with gain matrices $K_e \in \mathbb{R}^{m\times m}, K_x \in \mathbb{R}^{m\times n_m}, K_u \in \mathbb{R}^{m\times q_m}$, and $K_s \in \mathbb{R}^{m\times n_a}$.

This control law can be expressed in a compact form:

$$u_{ASC}(t) = K_a(t)r_a(t). \quad (8)$$

where the adaptive gain matrix evolves according to:

$$K_a(t) = K_P(t) + K_I(t). \quad (9)$$

The adaptation mechanisms are structured as:

$$K_P(t) = e_a(t)r_a^T(t)T_p. \quad (10)$$

$$\dot{K}_I(t) = e_a(t)r_a^T(t)T_I \quad (11)$$

with tuning matrices:

$$\begin{aligned} T_p &= \operatorname{diag}\left(T_{p_e}, T_{P_x}, T_{p_u}, T_{p_s}\right) \\ T_I &= \operatorname{diag}\left(T_{I_e}, T_{I_x}, T_{I_u}, T_{I_s}\right) \end{aligned}. \quad (12)$$

The complete basic structure of the proposed control method is illustrated in Fig. 2.

3.1 ERROR DYNAMICS, IDEAL CONTROL, AND STATE TRAJECTORIES

For good tracking at time t^*, the system output $y_a(t)$ should match the best model output $y_m(t)$

$$y_a^*(t) = C_a x_a^*(t) = C_m x_m = y_m. \quad (13)$$

Consequently, the tracking error vanishes:

$$e_a(t) = y_m(t) - y_a(t) = 0 \quad (14)$$

Define the ideal plant moving along bounded trajectories

$x_a^*(t) \in \mathbb{R}^n$

$$\begin{aligned} \dot{x}_a^*(t) &= A_a(x^*)x_a^*(t) + B_a(x^*)u_p^*(t) \\ y_a^*(t) &= C_a x_a^*(t) \end{aligned} \quad (15)$$

The control law is given by:

$$u^*(t) = \widetilde{K}_x x_m(t) + \widetilde{K}_u u_m(t) + \widetilde{K}_s x_a(t) \quad (16)$$

where $\widetilde{K}_x \in \mathbb{R}^{m\times n_m}, \widetilde{K}_s \in \mathbb{R}^{m\times n_a}$, and $\widetilde{K}_u \in \mathbb{R}^{m\times q_m}$ represent the ideal feedforward gains.

The state error is defined by: $e_x(t) = x_a^*(t) - x_a(t)$, the output error $e_a(t) = C_a e_x(t)$, taking into account the time derivative of the state error and substituting the ideal control from eq (16) also the actual control from equation (8), we obtain [16]:

$$\dot{e}_x = A_c e_x - B_a(x_a)K_p r_a - B_a(x_a)\big(K_I - \tilde{K}_a\big)r_a + R \quad (17)$$

where $A_c = A_a(x_a) - B_a(x_a)\widetilde{K}_e C_a, \widetilde{K}_a = \left[\widetilde{K}_e \widetilde{K}_x \widetilde{K}_u \widetilde{K}_s\right]$, and the residual term $R = J_F(x^*)e_x$ [16].

3.2 STABILITY ANALYSIS

Theorem 1. The application of the proposed adaptive synergetic control law, along with its associated adaptation mechanisms, to the augmented nonlinear system ensures the asymptotic convergence of tracking errors and bounded adaptive gains.

Proof. Consider the Lyapunov function candidate:

$$\begin{aligned} V(e_x, \varphi, K_I) = \; & e_x^T P(x_a)e_x + \varphi(e_a)^T\varphi(e_a) \\ & + \text{tr}\left\{\big(K_I - \widetilde{K}\big)T_I^{-1}\big(K_I - \widetilde{K}\big)^T\right\} \\ & + \text{tr}\left\{\big(K_I - \widetilde{K}\big)C_a B_a T_I^{-1}\big(K_I - \widetilde{K}\big)^T\right\} \end{aligned} \quad (18)$$

where $P(x_a) > 0$. Note that $V(0,0,\widetilde{K}) = 0$, $V(e_x, \varphi, K_I) > 0$ for all $\{e_x, \varphi, K_I\} \neq (0,0,\widetilde{K})$, and $V(e_x, \varphi, K_I) \to \infty$ if $\|e_x\| \to \infty, \| \varphi \| \to \infty$, or $\|K_I\| \to \infty$. The time derivative of $V(e_x, \varphi, K_I)$ is:

$$\begin{aligned} \dot{V} = \; & \dot{e}_x^T P(x_a)e_x + e_x^T \dot{P}(x_a)e_x + e_x^T P(x_a)\dot{e}_x \\ & + 2\varphi^T(e_a)\dot{\varphi}(e_a) + 2\text{tr}\left\{\big(K_I - \widetilde{K}\big)T_I^{-1}\dot{K}_I^T\right\} \\ & + 2\text{tr}\left\{\big(K_I - \widetilde{K}\big)C_a B_a T_I^{-1}\dot{K}_I^T\right\} \end{aligned} \quad (19)$$

where $V \equiv V(e_x, \varphi, K_I)$. Substituting $\dot{e}_x$ from eq. (17), $K_p$and $\dot{K}_I$ from eq. (10) and eq. (11), using the passivity relation, and performing the calculations, we get:

$$\begin{aligned} \dot{V} = \; & -2e_a^T e_a r_a^T T_p r_a - 2e_a^T C_a B_a e_a r_a^T T_p r_a \\ & - e_x^T\big[Q(x_a) + 2C_a^T T^{-1} C_a - 2P(x_a)J_F(x^*)\big]e_x \end{aligned} \quad (20)$$

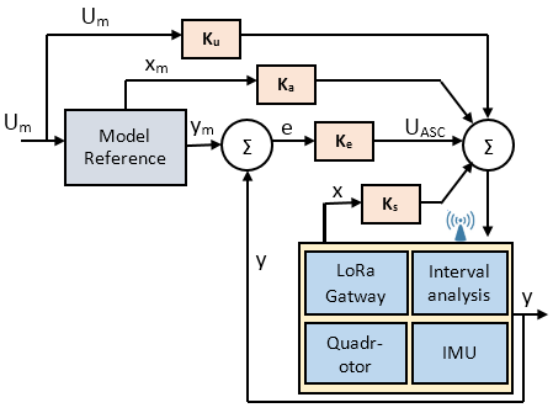

Fig. 2 – Control loop.

According to [16], for a Lyapunov derivative of the form eq. (24), the entire state $[e_x, \varphi, K_I]$ eventually reaches the domain $\Omega_f = \Omega_0 \cap \Omega$, where Ω is defined as $\dot{V}([e_x, \varphi, K_I(t)] \equiv 0)$ and $\Omega_0 = \{[e_x, \varphi, K_I] \mid V([e_x, \varphi, K_I(t)], t) \leq V([e_{x_0}, \varphi_0, K_{I_0}], 0)\}$ is the domain containing the system trajectories. Since $\dot{V}([e_x, \varphi, K_I(t)], t) < 0$ for e_x, the system eventually satisfies $e_x \equiv 0 \Rightarrow e_x(t) = 0 \Rightarrow e_a(t) = 0$. Thus, the asymptotic stability of the state and output tracking errors is guaranteed.

3.3 LORA COMMUNICATION TECHNOLOGY

LoRa communication technology enables long-distance, low-data-rate communication between the drone and base stations. The specific parameters associated with LoRa technology are highly dependent on modulation characteristics and configuration parameters.

The properties of LoRa technology, notably its low data rate wireless communications, which aim to cover long distances while maintaining low power consumption, make LoRa particularly suitable for Internet of Things (IoT) applications. While LoRa establishes the characteristics of the physical layer, LoRaWAN defines the system architecture and network protocols for LoRa-enabled devices. Specifically, via LoRa modulation, LoRaWAN offers medium access control (MAC), enabling LoRa end devices to communicate with a LoRa gateway [10].

3.3.1 CHANNEL MODEL

The characterization of a Radio channel in a specific environment can be expressed as a relationship between the distance between two radio stations and the RSSI value, where the relationship is [11-14]:

$$\text{RSSI} = -(10 \cdot n \cdot \log_{10}\, d - A) \quad (21)$$

where A represent the received power in dBm when the distance between the receiver and transmitter antenna is about 1m, and n is the loss exponent of the specific environment. The distance d is calculated as

$$d = 10^{\left(\frac{A-RSSI}{10.n}\right)}. \quad (22)$$

The parameter A is related to the physical properties of the radio device, while the value n heavily depends on the environment and the operating frequency. Equation (22) may be applied only under the ideal free space c-ndition, perfect with alignment and polarization of the antennas, and without path-loss and fading effects. However, the model is still valid in real world scenarios.

Since the parameter A depends on specific hardware characteristics and transmission conditions, a calibration step is required to determine its value empirically. In this case, parameter A was obtained by measuring the average RSSI value at a known distance of 1 meter between transmitter and receiver, in the real environment. This calibration enhances the accuracy of the distance estimate through eq. (22).

4. INTERVAL ANALYSIS

Measurements of RSSI values are subject to uncertainties that are either due to the measurements themselves or to various factors such as environmental noise, interference and

antenna variations. To optimize these uncertainties, the interval analysis technique is used. This method involves expressing distances as intervals that capture the uncertainty of the measurement. If ΔRSSI represents the measurement uncertainty RSSI, minimum distances $d_{\min}$ and maximum $d_{\max}$ can be calculated as follows [12] :

$$d_{\min} = 10^{\frac{P_t-(P_r+\Delta\text{RSSI})}{10\cdot n}} \cdot \quad d_{\max} = 10^{\frac{P_t-(P_r-\Delta\text{RSSI})}{10\cdot n}} \tag{23}$$

These intervals define a range of possible positions for the drone, reducing the impact of measurement uncertainty. The intersection of these intervals determines the drone's estimated position interval. For each base transceiver stations (BTS) i with position (x_i, y_i), position intervals can be found by solving

$$\text{Int X: } \left[x_i - d_{\max_i}, x_i + d_{\max_i}\right] \cap \left[x_i - d_{\min_i}, x_i + d_{\min_i}\right]$$
$$\text{Int Y: } \left[y_i - d_{\max_i}, y_i + d_{\max_i}\right] \cap \left[y_i - d_{\min_i}, y_i + d_{\min_i}\right] \tag{24}$$

The UAV position estimate is obtained by taking the average of the resulting X and Y intervals. The localization error is defined as the distance between the actual position and the estimated position of the UAV [17]:

$$\text{Error } = \sqrt{(x_{\text{real}} - x_{\text{estimated}})^2 + (y_{\text{real}} - y_{\text{estimated}})^2} \tag{25}$$

The performance of different BTS configurations is compared in terms of mean localization error and associated confidence intervals.

5. SIMULATION AND EXPERIMENTAL RESULTS

In this study, the simulation was carried out using MATLAB software. The platform used in the experimental tests is shown in Fig. 3.

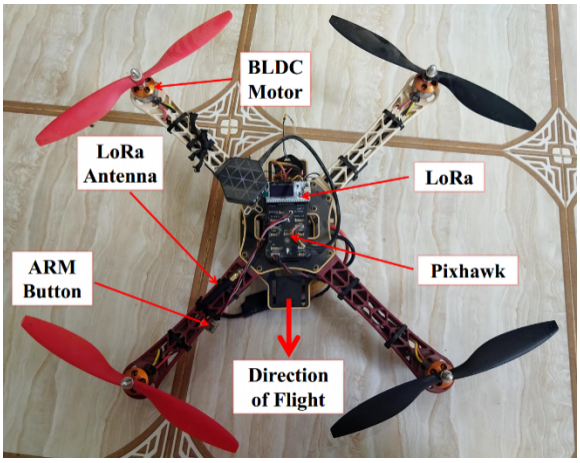

Fig. 3 – Drone with LoRa antennas.

This platform is equipped with a PX4 autopilot based on a 32-bit STM32F427 Cortex M4 core.

The embedded system contains a 6-DoF accelerometer/Gyro MPU-6000 and an STMicro LSM303D, a 3-axis accelerometer/magnetometer, as shown in Fig. 4.

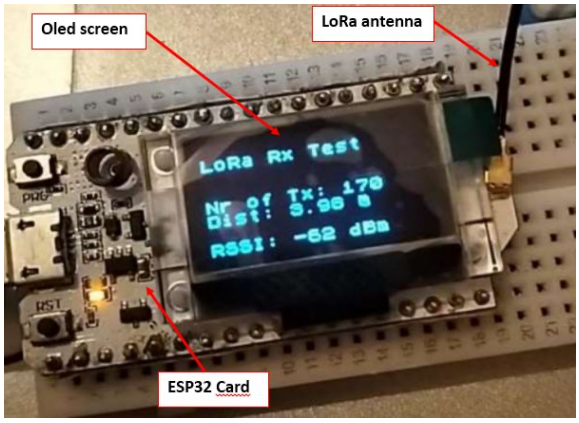

Fig. 4 – Tests for measuring distance using LoRa and RSSI.

The model parameters of the Quadrotor used are shown in Table 1.

Table 1

Table of Quadrotor parameters and their values.

Parameter	Value	Unit (mksA)
m	0.65	kg
I_x	0.011	kg m^2
I_y	0.036	kg m^2
I_z	0.029	kg m^2
b	3.13e^{-5}	N s^2
d	7.5e^{-7}	Nms^2
J_r	6e^{-5}	kg m^2
l	0.23	m

In Fig. 5, the drone is localized using three BTSs. The use of three BTSs significantly reduces the area of uncertainty where distance intervals overlap, enabling a more accurate estimation of the drone's position. This shows a significant improvement in localization accuracy compared with a two BTSs configuration, although some uncertainties remain. The localization error is lower, illustrating the positive impact of increasing the number of reference points on estimation accuracy.

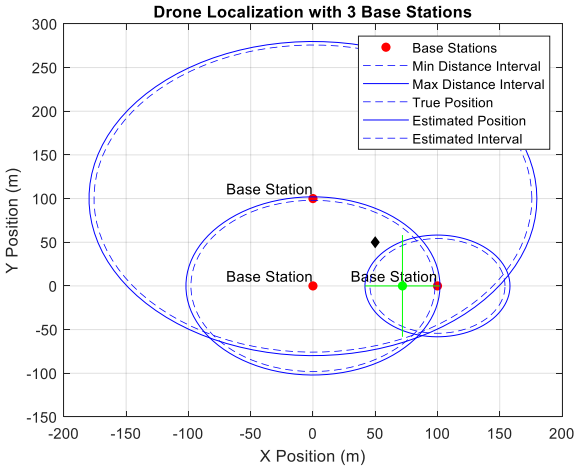

Fig. 5 – Localization with 3 BTSs.

Figure 6 uses localization with four BTSs, the area of uncertainty is considerably reduced, enabling a much more accurate estimation of the drone's position. The distance intervals overlap minimally, reducing the localization error to a very low level, close to zero. This configuration demonstrates the maximum effectiveness of localization techniques when the number of BTSs is sufficient to provide

redundant data and reduce uncertainties.

Figure 7 compares localization errors for configure-tins with 2, 3 and 4 BTSs, represented by vertical bars. The figure shows an apparent and progressive decrease in localization error as the number of BTS increases. With 2 BTSs, the error is highest due to large areas of uncertainty. With 3 BTSs, the error decreases considerably, and with 4 BTSs, the error becomes minimal.

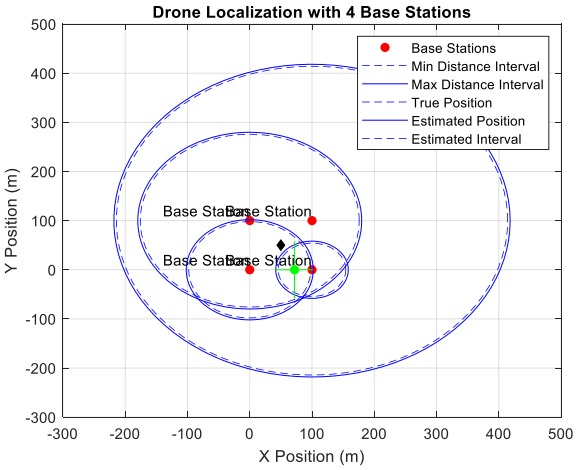

Fig. 6 – Localization with 4 BTSs.

This comparison highlights the importance of using more BTS to improve localization accuracy. It also illustrates how interval analysis techniques, when combined with redundant data from multiple sources, can minimize errors and improve the reliability of position estimates.

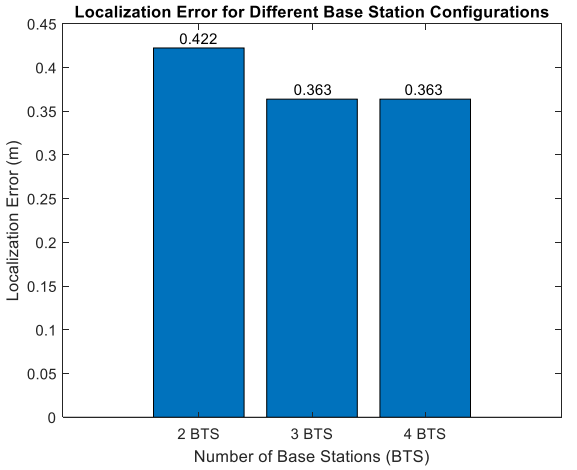

Fig. 7 – Error of localization.

Table 2 shows a significant improvement in localization accuracy compared to the method of [18]. This underlines the effectiveness of the proposed interval approach, even with a reduced number of BTSs.

Table 2

Comparison of the localization error to that of [18].

	2 BTSs	3 BTSs	4 BTSs	Work of [18]
Error (m)	0.422	0.363	0.363	0.92

Figure 8 shows the results of the system simulation. The first three graphs show the evolution of the Euler angles (roll, pitch and yaw) over time. The next three show the system's position in space (*x, y, z*). The seventh and eighth graphs show angular and position errors respectively. Finally, the last graph shows the control signals $u_{1,2,3,4}$ as a function of time.

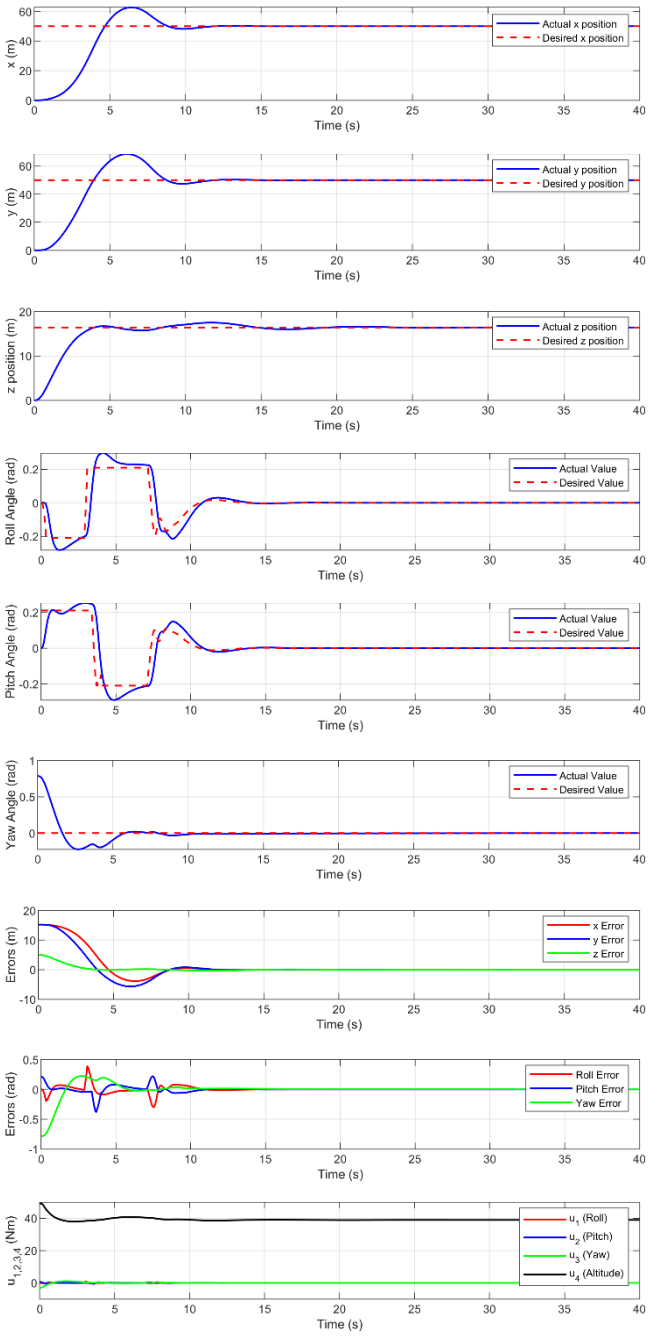

Fig. 8 – Control and stability results.

6. CONCLUSION

The approach proposed in this study combines LoRa communication technology, interval analysis, and passive adaptive control to offer an innovative and robust solution dedicated to UAV localization and control. Thanks to interval analysis, the method guarantees more accurate localization even in the presence of measurement uncertainties. At the same time, the use of adaptive control ensures system stability and self-adaptation to dynamic variations and disturbances. This robustness is essential for critical missions. One of the strengths of this approach lies in its enhanced resilience to adverse external conditions. The

system maintains a stable trajectory and satisfactory operational performance. This makes it particularly suited to applications in hostile or unpredictable environments.

CREDIT AUTHORSHIP CONTRIBUTION STATEMENT

Fawzi Srairi: Conceptualization and study design.
Khalil Mokhtar: Experimental tests and data acquisition.
Kheireddine Chara: Literature review and investigation.
Kamel Srairi: Original manuscript preparation and organization.
Mohamed Benbouzid: Review and manuscript editing.

Received on 3 November 2024

REFERENCES

1. C. Kheireddine, A. Yassine, S. Fawzi, M. Khalil, *A robust synergetic controller for Quadrotor obstacle avoidance using Bézier curve versus B-spline trajectory generation*, Intelligent Service Robotics, **15**, pp. 143–152 (2022).
2. L. Crupi, A. Giusti, D. Palossi, *High-throughput visual nano-drone to nano-drone relative localization using onboard fully convolutional networks*, In Proc. IEEE Int. Conf. Robot. Autom. (ICRA) (2024).
3. P. Nguyen, T. Kim, J. Miao, D. Hesselius, *Towards RF-based localization of a drone and its controller*, In Proc. ACM DroNet'19, Seoul, Republic of Korea (2019).
4. B. Kaplan, I. Kahraman, A.R. Ekti, S. Yarkan, A. Görçin, M.K. Ozdemir, H.A. Çırpan, *Detection, identification, and direction of arrival estimation of drone FHSS signals with uniform linear antenna array*, IEEE Access, **9**, pp. 152057–152069 (Nov. 2021).
5. H. Feroura, F. Krim, B. Talbi, A. Laib, A. Belaout, *Sensorless field-oriented control of current source inverter fed induction motor drive*, Rev. Roum. Sci. Techn. – Électrotechn. et Énerg., **63**, *1*, pp. 100–105 (2018).
6. P.-S. Wang, C.-H. Lin, C.-T. Chuang, *Real-time object localization using a fuzzy controller for a vision-based drone*, *Inventions*, **9**, pp. 14 (2024).
7. S. Ghosh, T.K. Saha, *Progressive step maximum power tracker for cascaded inverter induction motor drive*, Rev. Roum. Sci. Techn.–Électrotechn. et Énerg., **69**, *1,* pp. 3–8 (2024).
8. A.P. Brîncoveanu, R. Plămănescu, A.-M. Dumitrescu, M. Albu, *Voltage variability assessment in power systems*, Rev. Roum. Sci. Techn.–Électrotechn. et Énerg., **69**, *2*, pp. 171–176 (2024).
9. S. Latreche, B. Babes, A. Bouafassa, *Design and real-time implementation of synergetic regulator for a DC-DC boost converter*, Rev. Roum. Sci. Techn. – Électrotechn. et Énerg., **69**, *3*, pp. 305–310 (2024).
10. N. Nurelmadina, M.K. Hasan, I. Memon, R.A. Saeed, K.A. Zainol Ariffin, E.S. Ali, et al., *A systematic review on cognitive radio in low power wide area network for industrial IoT applications*, Sustainability, **13**, *1*, p. 338 (2021).
11. K.F. Haque, A. Abdelgawad, V.P. Yanambaka, K. Yelamarthi, *LoRa architecture for V2X communication: An experimental evaluation with vehicles on the move*, Sensors, **20**, *23*, pp. 6876 (2020).
12. T. Jian Ng, N. Kumar, M. Othman, *LoRa-based indoor positioning in dynamic industrial environments using deep Gaussian process regression and temporal-based enhancements*, IEEE Access, **12**, pp. 165298–165313 (2024),
13. E.D. Ayele, C. Hakkenberg, J.P. Meijers, K. Zhang, N. Meratnia, P.J. Havinga, *Performance analysis of LoRa radio for an indoor IoT application*, 2017 International Conference on Internet of Things for the Global Community (IoTGC), pp. 1–8 (2017).
14. M.I. Mahmud, A. Abdelgawad, V.P. Yanambaka, K. Yelamarthi, *Packet drop and RSSI evaluation for LoRa: An indoor application perspective*, IEEE 7th World Forum on Internet of Things (WF-IoT), pp. 913–914 (2021).
15. K. Mokhtari, M. Abdelaziz, *Passivity-based simple adaptive control for quadrotor helicopter in the presence of actuator dynamics*, IEEE 8th International Conference on Modelling, Identification and Control (ICMIC 2016), pp. 15-17 (Nov 2016).
16. K. Mokhtari, A. Elhadri, M. Abdelaziz. *A passivity-based simple adaptive synergetic control for a class of nonlinear systems*, Int. J. Adapt Control Signal Process, pp.1–15 (2019).
17. M. Filić, R. Filjar, M. Ševrović, *Expression of GNSS* positioning error in terms of distance, Promet – Traffic & Transportation, **30**, *3,* pp. 305–310 (2018).
18. G. Tian, D. Pjanić, X. Cai, B. Bernhardsson, F. Tufvesson, *Attention-aided outdoor localization in commercial 5G NR systems*, IEEE Transactions on Machine Learning in Communications and Networking (2024).